Fusion Engineering and Design 203 (2024) 114429

Contents lists available at ScienceDirect

Fusion Engineering and Design

journal homepage: www.elsevier.com/locate/fusengdes

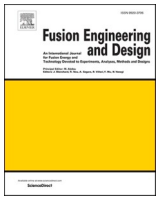

Design progress of DTT divertor fixation system

D. Marzullo [a,b], N. Massanova [a,b,*], F. Giorgetti [c,d], B. Riccardi [c], G. De Sano [d,e], S. Roccella [c,d]

[a] Department of Engineering and Architecture, University of Trieste, Via Alfonso Valerio, 6/1, Trieste 34127, Italy
[b] Consorzio CREATE, Via Claudio 21, Napoli 80125, Italy
[c] DTT S.C.a r.l., Via E. Fermi 45, I-00044 Frascati RM, Italy
[d] ENEA, Fusion and Technology for Nuclear Safety and Security Department, ENEA C. R. Frascati, via E. Fermi 45, Frascati 00044, Italy
[e] University of Rome Tor Vergata, Via Cracovia n.50 00133 Roma, Italy

ARTICLE INFO

Keywords:
DTT
Divertor
Concept design
FEA

One of the main challenges for the construction of DEMO, the first fusion demonstration reactor, is the power exhaust issue. To deal with it, EUROfusion has undertaken the construction of DTT (Divertor Tokamak Test) facility which will be held in Frascati, Italy. It aims to test various divertor models which can be integrated and used under different plasma confinement configurations. The current design of DTT embed 54 divertor cassettes which must be anchored to the vacuum vessel using suitable fixation systems. This paper deals with the initial monotonic load assessment of the fixation system of the Fixation System which must ensure compliance with multiple design requirements. The Remote Handling compatibility is one of the most demanding, since it includes a preloading phase of the divertor necessary to mitigate the shaking of the cassette due to dynamic forces. Moreover, the system must withstand the conspicuous loads acting on the Divertor due to the full or partial loss of plasma confinement (Disruptive Events). Structural verifications through Finite Element Method (FEM) have been performed on the Divertor-Fixation System, considering a set of load combinations, with particular focus on the most demanding case related to Fast-transient Vertical Disruption Event-downward.

1. Introduction

As in the majority of the experimental reactor, working under divertor magnetic configuration, the power issue exhaust is one of the most critical challenges to deal with. At DTT project core resides the divertor development [1], since the main aim of the project is to test different divertor shapes and different magnetic configuration in order to gain knowledges regarding the divertor performances [2]. Several challenges have to be faced during the design of the various sub system integrated into the divertor module. Among them disruption events stand out as the most demanding challenge [3]. Disruptions are sudden and violent occurrences within a plasma confinement device, characterized by the rapid release of energy and magnetic instability. These disruptive events subject the divertor system to extreme and often unanticipated thermal and mechanical loads. In these scenarios, the divertor components are exposed to a range of formidable conditions, including intense heat fluxes, extreme radiation, and severe electromagnetic forces. These disruptive forces can lead to material erosion, degradation, and potential structural damage. From the thermal load side, during normal operation, the plasma-facing surfaces of the Inner Vertical Target (IVT), and Outer Vertical Target (OVT), conditions are exposed to a substantial heat load which goes up to 20 MW/m^2 [1]. This delicate equilibrium between heat deposition, temperature fluctuations, and material response is vital to sustain the divertor structural integrity under regular operating conditions. In addition to standard operation, baking processes are an essential part of divertor maintenance. Two distinct baking conditions, Light Baking (LBK) at 200 °C and Severe Baking (SBK) at 240 °C, are used to ensure the optimal functioning of the divertor. These baking procedures introduce further challenges in terms of thermal loading and their impact on the mechanical properties of the divertor components. In this context, the divertor cassette-to-VV fixation system plays a major role since has to (indirectly) address all the challenges mentioned before, ensuring the stability of the divertor structure under each load condition (main dimensioning loads discussed in Section 3.1). The present paper reports the latest advancement in the design process of DTT divertor fixation system, starting from the modeling of the baseline solution up to the preliminary assessment of the design adopting, as reference rule, Structural Design Criteria for ITER In-vessel Components (SDC-IC) [4].

* Corresponding author.
E-mail address: nicola.massanova@phd.units.it (N. Massanova).

https://doi.org/10.1016/j.fusengdes.2024.114429
Received 13 October 2023; Received in revised form 22 March 2024; Accepted 4 April 2024
Available online 20 April 2024

Fig. 1. Divertor Design Overview.

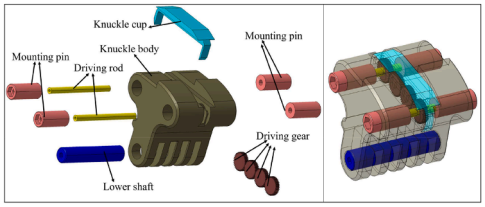

Fig. 2. Knuckle device components.

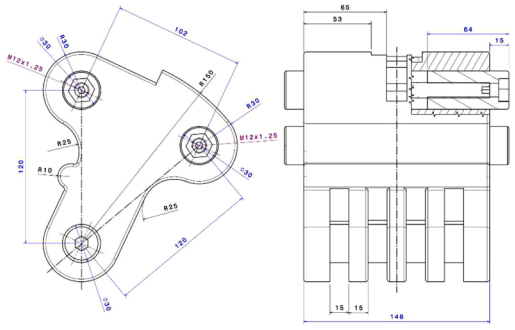

Fig. 3. Dimensions adopted for knuckle design (highlighted in blue).

2. Broad description of DTT divertor -to-vacuum-vessel fixation system

The actual baseline of DTT divertor fixation system has been designed following an ITER-like configuration [5]. Therefore, on the inboard divertor side a supporting structure called "nose" has been integrated on the current divertor Cassette Body (CB) design, while on the outboard side of the CB a device similar to the ITER knuckle [6] (in terms of overall behavior and assembly components) has been implemented (Fig.1).

2.1. Divertor fixation system design requirements

The design of the DTT divertor fixation system is based mainly on the following high-level requirements [7]:

Accordingly, main design parameters have been defined, as shown in Section 2.2, to fulfill design requirements and optimize the main dimensions.

2.2. Design methodology and components description

The main functional components, as well as the adopted materials, of DTT divertor fixation system are listed in Table 2.

Knuckle body is provided by a series of features which can host the other component embedded on it (Fig. 2). The mounting pin are hollow cylinders, whose inner surface is threaded and screwed on the driving rod. Therefore, by rotating the driving rod the pins displace towards their mounting holes. The driving gears link the rotation of the rear driving rod (which is actuated during the engagement operations) to the front one. The lower shaft will be rigidly connected to knuckle body, by mean of bolted connections, not yet integrated into the CAD model; therefore, the whole device can be rotated around its axis.

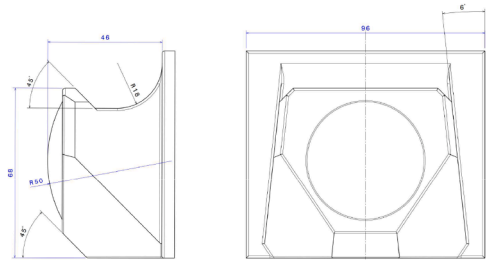

Fig. 4. Parameters adopted for nose design (highlighted in blue).

Table 1
High-Level Requirements DTT divertor fixation system.

Requirement ID	Descriptions
RQT_DIV-C-FS_#01	The fixation system shall lock the divertor cassette to the vacuum vessel
RQT_DIV-C-FS_#02	The fixation system shall be designed to carry the maximum HALO and eddy currents during the Vertical Displacement Events (VDE)
RQT_DIV-C-FS_#03	The fixation system shall ensure alignment of the divertor to the vacuum vessel during operation within $\pm$ 1.5 *mm*
RQT_DIV-C-FS_#04	The fixation system shall accommodate distortions and differential thermal expansion of the rail and the cassette
RQT_DIV-C-FS_#05	The fixation system shall withstand the electromagnetic loads specified in the Load Specification
RQT_DIV-C-FS_#06	The fixation system shall be totally compatible with the remote handling tools involved during the divertor installation
RQT_DIV-C-FS_#07	The fixation system shall ensure the electrical contact between the components in touch, in any condition

Table 2
DTT divertor fixation system components and materials.

Component	Material	Notes
Knuckle body	Ni-AlBr	The material has been selected for anti-seizure properties proven also in vacuum, high mechanical properties, low friction, spark resistance and low cost. It is available from stock as round forged bars its low friction properties
Driving rod	Ni-AlBr alloy	
Driving gear	Ni-AlBr alloy	
Knuckle cup	Ni-AlBr alloy	
Nose	Ni-AlBr alloy	
Mounting pin	Inconel 718	The material has been selected for its high mechanical and thermal properties
Lower shaft	Inconel 718	

The fixation system has been modeled through a parametric approach to facilitate the eventual modification of the geometrical features of the system. In following a top-down design [8] strategy, firstly the skeleton (or master model) of knuckle device and its divertor interface has been defined. The functional relationship, constraints, parameters, reference geometrical entities etc. have been implemented in it, aiming to facilitate the control of the dimensions and behavior of the components, ensuring consistency throughout the design. Fig. 3 shows, highlighted in blue, the dimensions which has been implemented as CATIA V5 parameters during the design.

The same approach has been adopted for the nose design (Fig. 4). The principal feature of the inner support is a hemispherical interface which, after the divertor engagement, is inserted in a socket on the inboard rail. The nose shape is designed to ensure the accurate toroidal centering of the pin-ball.

Fig. 5. Divertor during toroidal handling.

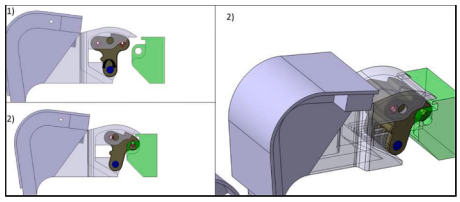

Fig. 6. Divertor in the proper toroidal position.

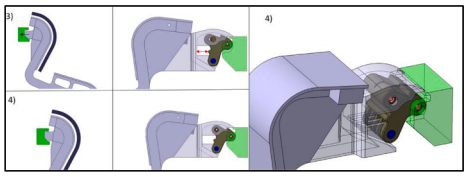

Fig. 7. Divertor preloading phase.

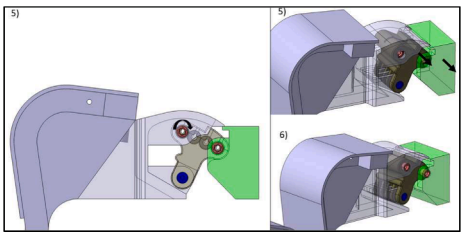

Fig. 8. Knuckle engagement.

2.3. Divertor mounting procedure

In the current paragraph, the mounting phases of DTT divertor are discussed. According to RQT_DIV-C-FS_#06 of Table 1, the cassette installation and RH compatibility is a main design driver for the fixation system. Thus, the mounting sequence and the RH tool availability greatly affects the design of the fixation system.

Similarly to ITER Divertor handling [9], the toroidal motion of each cassette is deployed to a robotic system called Cassette Toroidal Mover (CTM), while the radial positioning and other different maneuvers are managed by the Cassette Multi-functional Mover (CMM).Further details on such robotic tools are provided in [10]. During the toroidal handling, knuckle is retracted in its case, to avoid any clashes whit other in vessel components (Fig. 5).

Once the CTM reaches the proper toroidal position for the handled cassette, the lower shaft is rotated by a suited tool embedded on CMM, and knuckle with (Step 1 Fig. 6) in The front part of Knuckle is matched with the suited outboard rail vertical interface (Step 2 in Fig. 6).In this phase the divertor is hold in position through two supports which the knuckle case features and which rest on the outboard rail. At the same time, on the inboard side. The divertor keeps its position through the lower surface of the nose, which rests on the inboard rail. Therefore, from this point, the divertor cassette is free from CMM and CTM.

The CMM places an actuator between knuckle and the divertor cassette body. The actuator pushes until knuckle matches the lower semi cylindrical slot on the outboard rail (Step 3 in Fig. 7). In a first phase the divertor cassette body rigidly translates, and the nose is engaged on the inboard rail. After it, the "real" preloading phase starts and it lasts until knuckle matches the suited complementary interface on the outboard rail while the pins align with their mounting holes (Step 4 in Fig. 7).

The rotation of the rear Driving Rod drives the rotation of the Driving Gears which rotates the front Driving Rod (Step 5 in Fig. 8). Therefore, just actuating the front Driving Rod, both front pins and rear pins are engaged in their mounting holes (Step 6 in Fig. 8).

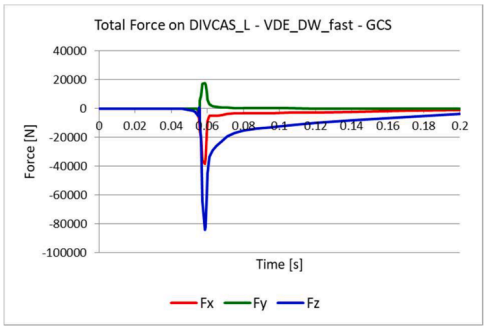

Fig. 9. EM forces resultants on Divertor Cassette body induced by 40 *ms* major DVDE.

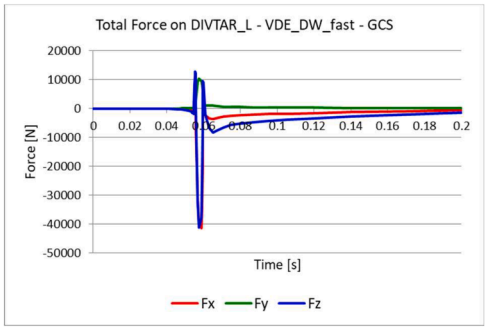

Fig. 10. EM forces resultants on VTs and DOME induced by 40 ***ms*** major DVDE.

3. FE structural assessment

3.1. Preload evaluation

Before delving deep into the analysis details, a premise is necessary. The preloading role is complex and involves several engineering and physical aspects. Said that, for its determination, in this work three aspects have been taken in account:

- The preload has to ensure that, under each load configurations (in particular during major VDE) the engagement of the divertor and its supporting structures is guaranteed.
- The preload has to compensate the effects of different thermal expansion between vessel and divertor

Therefore, considering the time history load (EM forces resultants on CB (Fig. 9) and forces resultants on VTs and Dome(Fig. 10)) of a major DVDE (40 *ms*), several trials have been done to understand which preload value could be more effective for the mentioned purposes.

In particular the force reaction of the contact between nose and inboard rail, along the preload direction has been investigated. The preload value which ensured that the force reaction component of the nose along the preload direction was always opposite to the preload during the whole analysis time (and therefore the nose keeps contact with the inboard rail) was 20 ***kN***. Therefore, the described analysis is related to a preload of 20 *kN*, which is the actual baseline value. The

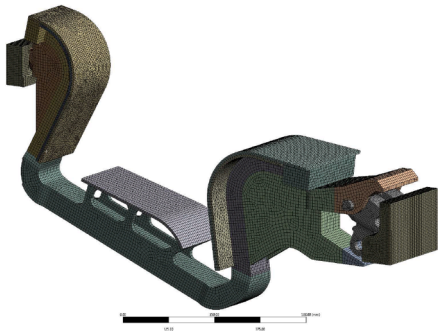

Fig. 11. Divertor mesh.

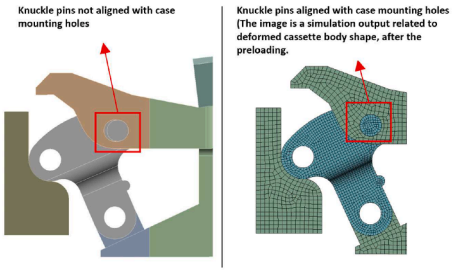

Fig. 12. Knuckle pins not aligned (left picture); Knuckle pins aligned (right picture).

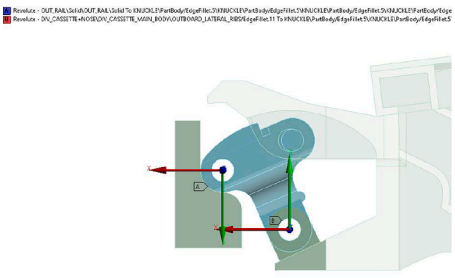

Fig. 13. Revolute joints set between knuckle and the surrounding components.

results in term of nose force reaction are reported in this section.

Fig. 11 shows the mesh of the model.

A dummy knuckle pin has been modeled to properly simulate knuckle engagement on the divertor cassette body after the preloading phase. In fact, the preloading force induces on the cassette body a maximum directional displacement (due to the compression/bending of the structure) which has been estimated to be of 4.8 *mm* using a preload value of 20 *kN*. To properly simulate the preloading phase, in SpaceClaim, the distance between inboard and outboard rail has been reduced by this value. During this procedure, the divertor cassette has been constrained to the supporting structures in accordance to the expected kinematic. Therefore, the geometry used as starting point for the analysis, had the dummy pin not aligned with their mounting holes as can be seen in Fig. 12. Once the preload action is exerted (through a joint load which will be described later) the pins align and the contact imposed between them and their holes activates.

The imposed set of connection is below outlined:

- A revolute joint has been imposed between the lower knuckle support holes and knuckle case hole interfaced with them (replacing the behavior (Fig. 13).

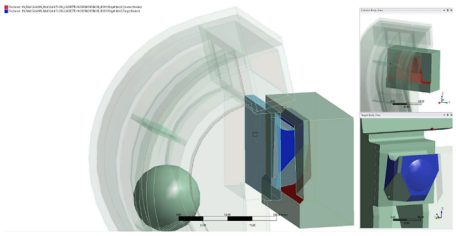

Fig. 14. Frictional contacts between nose and inboard rail.

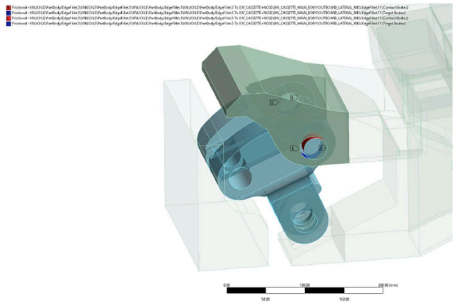

Fig. 15. Frictional contact between knuckle dummy pins and knuckle case.

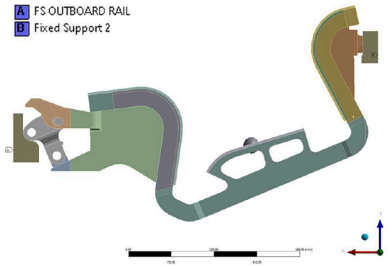

Fig. 16. Fixed supports set on inboard rail and nose.

- A revolute joint has been imposed between the front knuckle holes and the cylindrical surface of the outboard rail (Fig. 13) (to simulate the behavior of the outer knuckle pin).
- Frictional contacts, shown in Fig. 14 have been imposed between nose and inboard rail surfaces (friction coefficient 0.2)
- Frictional contacts have been imposed between knuckle and knuckle case (friction coefficient 0.2)
- A frictional contact has been imposed between the dummy pins and knuckle case holes interfaced with them (friction coefficient 0.2) (Fig. 15)

Both outboard and inner rail have been grounded through a fixed support set on their outer surfaces (Fig. 16).

The analysis has been conducted as multistep:

- Step 1 ($0\ s - 1\ s$): Joint load on the lower shaft joint (3.1°imposed). The joint load act as preloading tool and its action will align the dummy pins with their respective knuckle case holes. As mentioned before the joint load value was directly related to the wanted preload value.
- Step 2 ($1s - 2\ s$) : Activation of the frictional contact between dummy pins and knuckle case holes (which are aligned after the preload)
- Step 3 ($2s - 3s$): Force gravity and thermal condition .A uniform temperature of 130 °C set on the whole CB structure, which is the higher operational temperature of the CB cooling water).

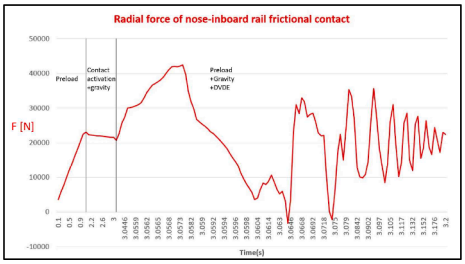

Fig. 17. $F(x)$ nose constraint reaction.

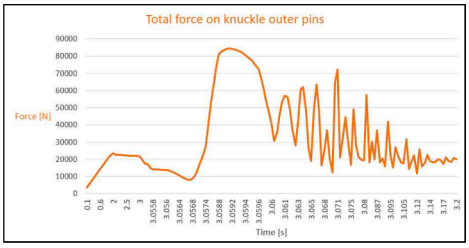

Fig. 18. Knuckle outer pin total constraint force (joint reaction).

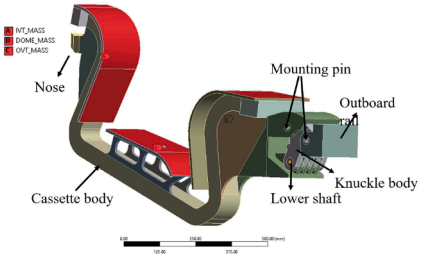

Fig. 19. Geometry included into the static global analysis.

In Step 4 to step 27 (Time $3s - 3.2s$), the resultant EM forces spectrum, induced by a major DVDE of 40 *ms* (on Divertor Cassette Body, Vertical Targets and Dome) has been implemented. The forces resultants have been applied as uniformly distributed nodal forces.

Fig. 17 shows the time plot of the X force reaction (preload direction) of the frictional contact between nose and inboard rail.

As can be seen, just during few instants of time the force reactions is slightly below zero. This result should not be misleading. In fact, although in those few instants of time the reaction has the same sign of the preload, the nose does not disengage thanks to the action of the hook which features.

In Fig. 18 is shown the trend of the force reactions on the revolute joint imposed between knuckle outer hole and the inboard rail holes.

In the next analysis which will be presented, the reaction forces acting on knuckle pins are reported. These are higher than the overtime maximum value of 85,340 N which occurs during the dynamic analysis described in this section. This is due to the constraining conditions of the divertor used for the analysis presented in Section 3.2 and also to the methodology used to apply the EM loads. Moreover, the effect of the preload seems to mitigate the constraint reaction acting on knuckle pin due to the EM loads. Therefore, the verification in Section 3.2 (in which a lower preload value has been used) is more conservative and has been used for the dimensioning and verification of knuckle pins.

3.2. Static global FE analysis

Aim of the analysis was to catch the overall behavior of the system under the loads. The CAD model has been defeatured by simplifying the features which were not relevant for the analysis purpose. The Plasma

Table 3
Divertor subsystem masses.

	CB+ Knuckle +Nose	OVT (A)	IVT (B)	DOME (C)	Tot
Mass [kg]	143	75	40	48	306

Table 4
Material, yield strength and minimum allowable stress of modeled components (S_Y and S_m took from [11]).

Component	Material	Sy [MPa] (130 °C)	Sm [MPa] (130 °C)
Knuckle body	NiAlBr Alloy	286	195
Mounting pins	Inconel 718	1049	425
Lower shaft	Inconel 718	1049	425
Cassette body	AISI 316 L IG	200	147
Outboard rail (dummy)	AISI 316 L IG	200	147
Nose	NiAlBr Alloy	286	195

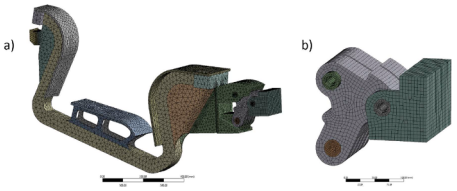

Fig. 20. a) Global model mesh-b) Knuckle components and dummy outboard rail mesh.

Facing Components were not considered in the presented analyses since their stiffness is almost negligible with respect to CB one. The Outer Vertical Target (OVT), Inner Vertical Target (IVT) and the DOME have been replaced by concentrated masses referred to the respective supports. In Fig. 19 the considered geometry is shown.

The mass of each divertor subsystem is outlined in Table 3.

In Table 4 the material of each considered component are listed, whose Young Modulus dependence [11] with temperature has been set in ANSYS Workbench Engineering Data.

The global analysis has been conducted with the main purpose of capturing the structural displacements which the model undergoes due to the imposed loads. Therefore, a coarse mesh has been generated on the cassette body, while the bodies in contact to each other, as knuckle or knuckle case, have been meshed using a smaller size, to avoid any contact issue. The mesh included 278,533 nodes and 106,028 elements (quadratic elements type). The meshed model is shown in Fig. 20 with a focus on knuckle assembly and the dummy outboard rail implemented into the simulation.

Frictional contacts have been set between the components where a relative sliding displacement was foreseen. Nose is mounted on the divertor thorough threaded connections. This connection has been simulated through a bonded contact, set between the rear surface of nose and the nose pad behind it. Since, as previously clarified, the lower shaft and knuckle body are rigidly connected, a bonded contact has been set between the surfaces of the lower shaft interfaced with knuckle body.

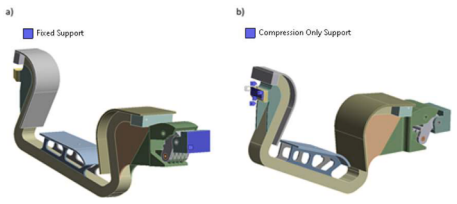

Fig. 21. a) Fixed support imposed on the outer surface of the outboard rail b) Compression only set on nose surfaces.

Table 5
Forces resultants on cassette body and PFCs.

	F_x [N]	F_y [N]	F_z [N]
CB	− 61,800	19,100	− 77,000
OVT	40,032	792,7	− 5041,5
IVT	− 88,857	− 464,2	9940,8
DOME	− 31,585	98,4	− 64,636

Table 6
Moments resultants with respect to the center of DTT machine.

	M_x [N∗mm]	M_y [N∗mm]	M_z [N∗mm]
CB	$5.45 * 10^7$	$2,04 * 10^8$	$5,34 * 10^6$
OVT	$4,41 * 10^5$	$-4.99 * 10^7$	$1,37 * 10^6$
IVT	$-6,21 * 10^4$	$8,96 * 10^7$	$-3,49 * 10^5$
DOME	$-6,33 * 10^5$	$1,65 * 10^8$	$1,42 * 10^4$

Therefore, the interaction between knuckle and outboard rail has been faced as a contact type issue. Differently, to simulate the behavior of the nose engaged on the inboard rail, a compression only boundary condition has been imposed. The compression only support has been referred to the functional surfaces of the nose which, after the preloading, are expected to be interfaced. The outboard rail design for the DTT tokamak is planned to consist of two separate components: a pad attached to the vacuum vessel by mean of welded ribs, and an intermediate component secured to the pad through bolted joints. For the analysis pursuit, as shown in Fig. 21, only the second one has been included. To simplify matters, the interaction between this component and the welded pad has been simulated using a straightforward fixed support that fully constrains the outer surface of the outboard rail. Fig. 21 shows the boundary conditions set in the model.

The analysis has been carried out as multistep. If not, the simultaneous concurrence of the loads implied into the simulation could have led to inconsistent results.

The analysis is linear elastic, thus the value of stresses above yield strength are not allowed for verification purposes. Progressively the complete load configuration has been set:

- STEP 1: Dead Weight
- STEP 2: Preload (4 kN)
- STEP 3: Downward Vertical Displacement Event (DVDE) induced Forces resultants
- STEP 4: Downward Vertical Displacement Event (DVDE) induced Moments resultants
- STEP 5: Uniform body temperature of 130 °C

The resultant EM loads come from the force elemental density distribution induced by a Fast Downward Vertical Displacement Event (DVDE fast) with current quench time of 40 ms. Among several loss of plasma scenarios studied, this has been identified as the most critical for the divertor. This is mainly due to the HALO currents contribution, which during a Slow DVDE induce huge loads on the divertor system. The instant of time (into the disruption scenario) in which the resultants of forces and moments were higher has been spotted. To set the loads, a remote point has been placed in DTT machine center and referred to the Cassette Body surfaces. The forces and moments resultants have been applied in such remote point (their components have been specified in a proper oriented Coordinate System, with origin in the machine center, the X axis along the radial direction, Y along toroidal, Z along vertical). The same has been done for the IVT, DOME, OVT support surfaces.

The defined EM loads are listed in Table 5 and Table 6.

The results in terms of displacement and stress contours are shown in Fig. 23 and Fig. 24. They are related to the last load step (Step 5), in which all the specified loads are considered.

As it can be seen in Fig. 25, the front mounting pins and the front region of knuckle body are the most stressed. Therefore, further investigations have been conducted, starting from the global analysis results.

3.3. Submodeling analysis

To evaluate with higher accuracy the stress state acting on the previously outlined regions, different submodeling analysis have been performed. No verification of nose has been carried out, since its design wasn't detailed enough. Since the submodeling procedure ensure reliable analysis results with less computational costs than a global analysis, this approach is widely adopted in engineering design of in-vessel components [12]. Generally, the submodeling procedure involves two steps. In the first one a global model, which uses a relatively coarse mesh to represent the entire geometry, is analyzed. While this global model may have significant errors in calculated results in certain localized regions, it still produces acceptable results for most of the geometry. In particular the stiffness properties, and consequentially the overall behavior in terms of displacement is quite reliable. On the other hand, the second model, known as the "sub-model," is designed to provide a much more detailed representation of specific regions of interest within the global model. These regions often involve phenomena like stress concentration. Traditionally, in structural mechanics applications, cut boundary conditions for the sub-model are determined by interpolating nodal displacements calculated by the global model onto the cut boundary nodes of the sub-model.

The idea is to cut the knuckle body, as close as possible to the outer part of the model (Fig. 26), to minimize loss of load information's. In the first submodeling analysis, the Front Upper Pins have been removed and substituted with cylindrical joints, in order to evaluate the shear constraint reactions and perform a preliminary hand calculation on them. The other imposed contacts have been kept the same. The global analysis has been linked to the submodeling and the displacements on the cut section have been imported and interpolated on the new mesh (Fig. 27). Since none of the other components of the global analysis has been kept into the submodeling simulation, it was possible to build a high-quality mesh (Fig. 26).

The pins were characterized by the following dimensions:

Using as input loads the constraint forces reactions, the shear stress acting on each pin has been evaluated:

- Shear stress on left mounting pin (in joint coordinate system *XY* plane):

$$\tau_{XY} = \frac{T_{tot}}{A} = \frac{T_{tot}}{\pi\left(\left(\frac{D}{2}\right)^2 - \left(\frac{d}{2}\right)^2\right)} = 1106MPa > S_{y_{Inconel718}}$$

- Shear stress on right mounting pin (in joint coordinate system *XY* plane):

$$\tau_{XY} = \frac{T_{tot}}{A} = \frac{T_{tot}}{\pi\left(\left(\frac{D}{2}\right)^2 - \left(\frac{d}{2}\right)^2\right)} = 1725\,MPa > S_{y_{Inconel718}}$$

After this preliminary submodeling which aimed to roughly estimate the shear stress on the pin, an additional submodeling analysis has been performed. In Fig. 29 the sub modeled geometry and its mesh can be seen.

In Fig. 30 is shown the imposed contacts set.

Fig. 31 shows the equivalent Von Mises stress acting on the model and its subcomponents.

To perform the verification on the mounting pins and on knuckle

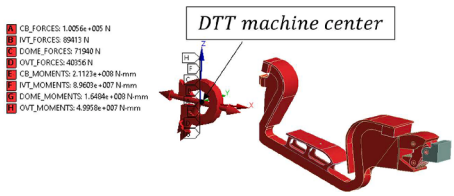

Fig. 22. EM loads configuration set on divertor.

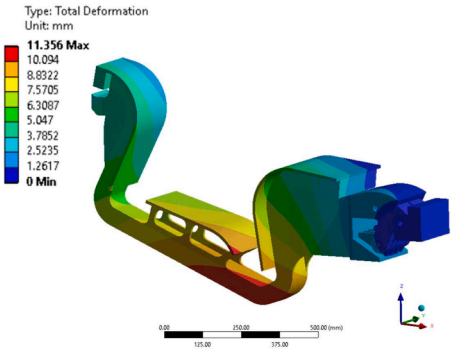

Fig. 23. Divertor Total displacement (maximum total displacement of 11.3 mm).

body front region, the stress, along several Stress Classification Lines has been probed. Each line was along the radial direction of the pins. Below are reported the verifications, carried out on the most critical paths, in compliance with [4]. The membrane component and membrane plus bending component of the Eq. von Mises Stress on point 1 of the Stress Classification Line (SCL) highlighted in the left mounting pin (Fig. 32a) were:

- Pm=748 MPa > Sm=425 MPa
- Pm +Pb=931.35 Mpa > 1.5 Sm=637.5 MPa

While for the point 1 of the SCL implemented on the right mounting pin (Fig. 32b):

- Pm=690.67 > Sm=425 Mpa
- Pm +Pb=1134.12 > 1.5 Sm=637.5 MPa

For both pins, the structural verification criteria were not met. Moreover, the stress acting on knuckle front region was way higher than the threshold set by the verification criteria, therefore the SCL construction and the stress linearization along it, is not reported. Anyway, iterative adjustments of pins dimensions have been done, until the verification was passed. Ultimately, by setting the external diameter at 40 mm and the inner diameter at 14 mm, the verification for both pins was successful.

The linearized Equivalent von Mises stress components on point 2 of SCL, for the left mounting pin (left in Fig. 33) were:

- Pm=282.12 MPa < Sm=425 Mpa
- Pm +Pb=345.83 MPa < 1.5 Sm=637.5 MPa

On point 1 of the SCL on the right mounting pin (right in Fig. 33):

- Pm=380.56 MPa < Sm=425 Mpa
- Pm +Pb=533.47 MPa < 1.5 Sm=637.5 MPa

Unlikely the knuckle body front region was characterized by stresses higher than the allowable. Either way, further modifications are foreseen to strengthen knuckle body design. The examination of stress trend

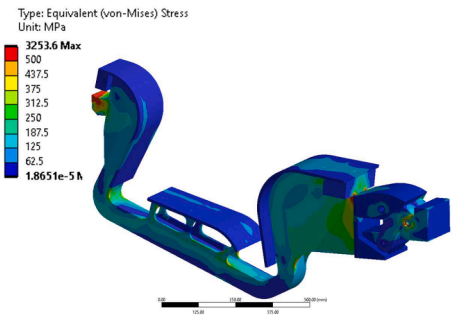

Fig. 24. Divertor equivalent Von Mises Stress (peak of 3253.6 ***MPa***).

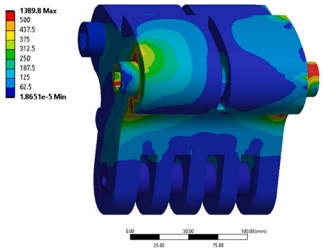

Fig. 25. Knuckle equivalent von Mises stress (peak of 1389 MPa).

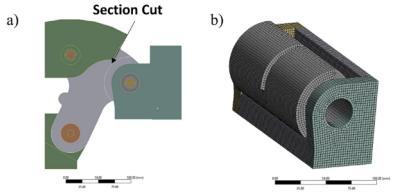

Fig. 26. a) Geometry included in the first submodeling analysis b) Mesh (78,744 elements and 330,255 nodes).

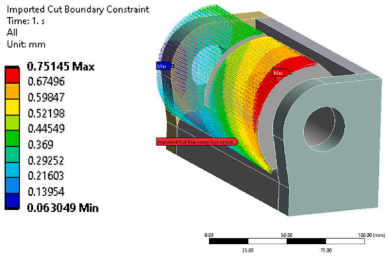

Fig. 27. Imported cut boundary displacements on section cut.

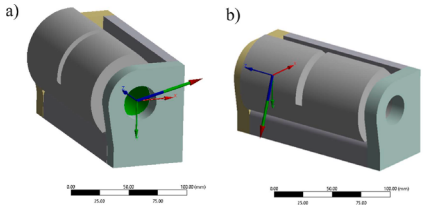

Fig. 28. Constraint forces reactions on left cylindrical joint a) and right one b).

on the nose has remained unexplored due to the inherent lack of refinement in its initial design, rendering it unsuitable for detailed analysis (Fig. 22,Fig. 28,Table 7,Table 8).

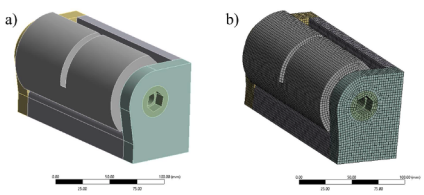

Fig. 29. a) Sub model b) Mesh (87,201 elements and 366,720 nodes).

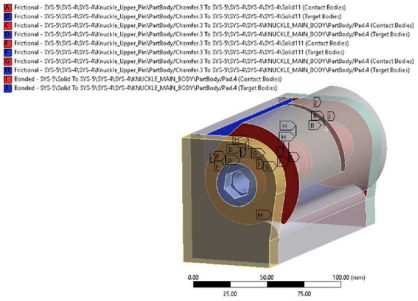

Fig. 30. Contact set between interfaced components (friction coefficients imposed in frictional contact of 0.2).

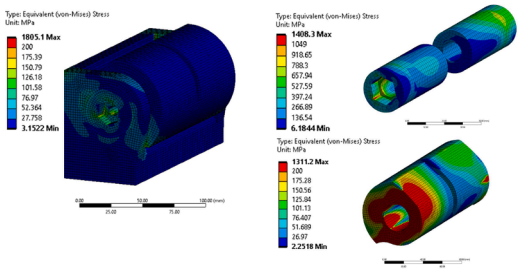

Fig. 31. Knuckle sub model equivalent Von Mises stress (peak of 1805 ***MPa*** occurring on the outboard rail).

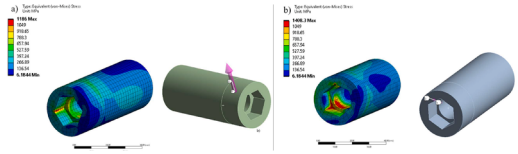

Fig. 32. a) Equivalent Von Mises stress and most critical SCL on left mounting pin (eq. Von Mises stress peak of 1186 ***MPa***) b) Equivalent Von Mises stress and most critical SCL on left mounting pin (eq. Von Mises stress peak of 1186 ***MPa***).

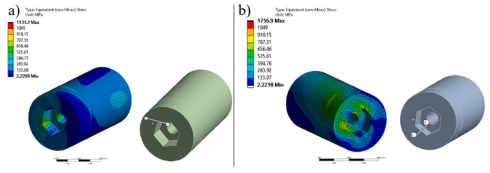

Fig. 33. a) Equivalent Von Mises and most critical SCL on right mounting pin (eq. Von Mises stress peak of 1131 ***MPa***) b) Equivalent Von Mises and most critical SCL on right mounting pin (eq. Von Mises stress peak of 1756 ***MPa***).

4. Conclusion

In this paper the design progress of DTT divertor fixation system have been discussed. Starting from the design of each component of the knuckle and nose, up to the verification and dimensioning of the main functional components of knuckle device, the mounting pins. Based on the analysis results outlined in Section 3.1, a preload of 20 kN has been identified as the actual baseline value. The paper presented an initial assessment of stress values for the fixation system, pending further studies based on the updated EM force density distribution calculated on the lates divertor geometry. The design work is still on going and further development are foreseen for the engineering design of the concept.

Table 7
Constraint forces reactions on left cylindrical joint.

(N)	$F_y\ (N)$	$F_z\ (N)$	$F_{tot}(N)$
$-1.98 * 10^5$	$5.8 * 10^5$	0	$6.1 * 10^5$

Table 8
Constraint forces reactions on right cylindrical joint.

(N)	$F_y\ (N)$	$F_z\ (N)$	$F_{tot}\ (N)$
$9.3 * 10^5$	$-2.2 * 10^5$	0	$9.5 * 10^5$

CRediT authorship contribution statement

D. Marzullo: Writing – review & editing, Writing – original draft, Visualization, Validation, Supervision, Project administration, Methodology, Investigation, Formal analysis, Data curation, Conceptualization. **N. Massanova:** Investigation, Formal analysis, Data curation, Conceptualization, Methodology, Validation, Visualization, Writing – original draft, Writing – review & editing. **F. Giorgetti:** Conceptualization, Supervision, Validation, Visualization. **B. Riccardi:** Conceptualization, Project administration, Supervision, Validation, Visualization. **G. De Sano:** Investigation, Visualization. **S. Roccella:** Conceptualization, Investigation, Methodology, Project administration, Supervision, Validation, Visualization.

Declaration of competing interest

The authors declare that they have no known competing financial interests or personal relationships that could have appeared to influence the work reported in this paper.

Data availability

Data will be made available on request.

References

[1] R. Albanese, WPDTT2 Team, DTT: a divertor tokamak test facility for the study of the power exhaust issues in view of DEMO, Nuclear Fusion 57 (1) (2016) 016010.
[2] G. Maddaluno, et al., The DTT device: Divertor solutions for alternative configurations including liquid metals, Fusion Engineering and Design 122 (2017) 341–348.
[3] F. Giorgetti, et al., Vertical displacement events analysis using MAXFEA code in combination with ANSYS APDL in the final design stage of the DTT vacuum vessel, Fusion Engineering and Design 184 (2022) 113273.
[4] In-vessel Components, SDC-IC (ITER private communication).
[5] V. Komarov, et al., Design progress of the ITER divertor cassette-to-vacuum vessel locking system, Fusion Engineering and Design 82 (15-24) (2007) 1866–1870.
[6] L. Guerrini, et al., Fabrication of ITER divertor Cassette body prototypes, Fusion Engineering and Design 162 (2021) 112054.
[7] F.G. Lanzotti et al., RFLP approach to DTT divertor fixation system design using the 3DExperience platform.
[8] R. Mozzillo, et al., Development of a master model concept for DEMO vacuum vessel, Fusion Engineering and Design 112 (2016) 497–504.
[9] A. Tesini, et al., The ITER remote maintenance system, Fusion Engineering and Design 83 (7-9) (2008) 810–816.
[10] C. Lauretti, et al., Remote Handling System for the DTT Fusion Reactor: A System Engineering Approach for Preliminary Conceptual Design of the Main Robotic

Equipment, in: Offshore Mediterranean Conference and Exhibition. OMC, 2021 p. OMC-2021-110.
[11] RCC-MRx, Design and construction rules for mechanical components of nuclear installations. AFCEN, 2012.
[12] P. Testoni, et al., A sub-modeling approach for the electromechanical disruption analysis of the ITER ICH antenna, Fusion Engineering and Design 83 (5-6) (2008) 695–701.